PPPL-2289

UC20-A,B,D,F

PPPL-2289

DISCHARGE CONTROL AND EVOLUTION IN TFTR

By

D. Mueller et al.

JANUARY 1986

PLASMA PHYSICS LABORATORY

PRINCETON UNIVERSITY

PRINCETON, NEW JERSEY

PREPARED FOR THE U.S. DEPARTMENT OF ENERGY,
UNDER CONTRACT DE-AC02-76-CHO-3073.

DISCHARGE CONTROL AND EVOLUTION IN TFTR

PPPL--2289

DE86 005359

D. Mueller, M. Bell, F. Boody, C. Bush[a], J.L. Cecchi,

S. Davis, H.F. Dylla, P.C. Efthimion, R.J. Hawryluk,

K.W. Hill, S. Kilpatrick, P.H LaMarche, D. Manos,

D. McCune, S.S. Medley, S. Milora[a], M. Murakami[a]

D.K. Owens, J. Schivell, G. Schmidt, S. Sesnic,

B. Stratton, G. Tait, M. Ulrickson, K.L. Wong,

R.D. Woolley, M.C. Zarnstorff

Princeton Plasma Physics Laboratory,

Princeton University

Princeton, New Jersey 08544 USA

INTRODUCTION

The Tokamak Fusion Test Reactor (TFTR) was designed to explore plasma confinement and heating at reactor-like parameters. Since the first plasma in December 1982, considerable progress has been made in this endeavor. During the run period ending April 13, 1985, operation of both the toroidal field and plasma current at full design parameters was achieved. The plasma parameters achieved are summarized in Table 1.

Control of the discharge evolution played an important role in achieving these parameters. The control of impurities in a tokamak is largely a result of the choice of limiter and wall materials, conditioning techniques and gettering. The impurity control procedures adopted during this run will be discussed first, because impurities play an important role in determining the operating limits. The discussion of discharge evolution and control will be

broken down into discharge initiation, volt-second consumption, and current and density ramp-up and ramp-down. Control of the current ramp-up using a plasma growing technique will be described and the advantages of this method compared to using constant major and minor radii will be discussed. The control of density using gas puffing, pellet injection, and neutral beam fueling will be presented along with a discussion of the density range which is found to increase with plasma current.

IMPURITY CONTROL

The operation of TFTR at low Z_{eff} and the extension of the density range have been made possible by the choice of limiter and wall materials, conditioning, and gettering. The TFTR vacuum vessel consists of 304LN stainless steel and Inconel 625 bellows.[1] The bellows are protected by Inconel X750 cover plates. These cover plates act as the limiter for small major radius plasmas ($2.1m < R < 2.48m$) and as protective armor for the bellows during disruptions. Water-cooled TiC- coated graphite tiles protect those portions of the outer wall subject to direct neutral beam bombardment. The moveable limiter on TFTR allows for a range of major and minor radii to be used in the investigation of size scaling experiments.[2] The limiter is comprised of three blades, a vertical blade on the large major radius side of the plasma and upper and lower blades hinged to the vertical blade. The vertical blade can be moved radially 0.17m. The upper and lower blades can be opened and closed to allow minor radii (a) between 0.83 and 0.25m at a major radius (R) of 2.55m. For given limiter positions a depends on R. For example, with the limiter fully opened at R=3.05m then a=0.55m and the plasma is in contact with all three blades. The limiter consists of water-cooled graphite tiles mounted on Inconel plates. The graphite tiles were originally

coated with TiC, but after four months of plasma operation it was found that this coating was severely damaged and the remaining TiC was removed.[3] The bare graphite limiter was used throughout the most recent run period. The removal of the TiC coating resulted in the reduction of the Ti concentration in the plasma by a factor of about 50.[4] As might be expected, operation with the Inconel bumper limiter results in plasmas with high metallic concentration and radiation.

With the plasma limited by the graphite limiter at R=2.55m, a=0.83m, the plasma boundary is about 0.1m from the Inconel cover plates. Motion of only 10mm inward from R=2.55m causes the radiated power to increase, while motion outward causes it to decrease. Figure 1 illustrates this effect for plasmas with different major radius programming during the current flattop of 1.4MA and with the density nearly constant. In general, the radiated power in discharges having constant radius and density during the current flattop reaches a peak near the beginning of the current flattop (1.5s for these discharges) then falls slowly. A 10mm step inward in major radius from 2.55m at 3 seconds causes the radiated power to increase by about 50kW, and moving the plasma out by 10mm from 2.55m at 3 seconds has the effect of lowering the radiated power by about 50kW. These changes in radiation were due to metals, primarily Ni. A likely source of Ni is the Inconel bumper limiter. Ramping the plasma in from R=2.64 to 2.53m caused the radiated power to increase above the level it would have been at constant radius when $R \lesssim 2.59$m. Infrared camera measurements of the moveable limiter[5] indicate a power scrapeoff length of 15mm. The probe measurements indicate a power scrapeoff thickness which evolves smoothly from a value of 30 to 40mm during the current ramp-up to 15mm during the flattop increasing to 25mm during the ramp-down. Both these measurements are considerably less than the distance from the nominal plasma

boundary to the wall. The choice of materials is clearly important even for structures several scrape-off lengths from the plasma boundary.

The purpose of conditioning is to remove impurities from the walls and limiters after a vacuum opening. Conditioning on TFTR has been achieved by a combination of bakeout of the vacuum vessel at 150C, glow discharge cleaning (GDC), pulse discharge cleaning (PDC) in both a high and low current mode to reduce low Z impurities and high power pulsing. The details of these discharge cleaning methods have been described by Dylla et al.[6,7] Table 2 gives the parameters used during discharge cleaning. The partial pressures of the background gas constituents (primarily CH_4, H_2O, and CO/C_2H_4) were measured by a residual gas analyzer.[8] Bakeout was effective in increasing the removal rate of these background gas constituents. During GDC the removal of impurities was further enhanced. The low current mode of PDC was more effective in removing impurities than was the high current mode. The high current mode of PDC was employed primarily to heat the limiter to 250C and enhance the effectiveness of the low current mode. This combination of discharge cleaning techniques was sufficient to allow operation of high power pulses.

Normal operation at low currents (I_p < 1.0MA) was performed after discharge cleaning before operation at higher currents was attempted. As each higher level of plasma current (typically ΔI_p=0.4MA) was attempted, the discharges showed signs of distress (increased loop voltage, and higher radiated power) for several shots. The fractional radiated power (P_{rad}/P_{OH}) fell during this conditioning period at each successively higher current. It is not clear if conditioning or operator experience contributed more to this initial improvement. However, an overall downward trend in P_{rad}/P_{OH} was observed for similar shots throughout most of the run period. Figure 2 shows

the nickel concentration in the plasma as measured by X-ray spectrometry for density scans at 1.0MA taken on different days. The nickel concentration dropped with the number of shots since PDC or since the production of plasmas on the Inconel bumper limiter. It appears that Ni is deposited on the moveable limiter during discharge cleaning and when the Inconel bumper limiter is employed, while normal operation on the moveable limiter removes the Ni. This is not meant to imply that the nickel radiation was a large part of the total radiated power. Calculations made using the code MIST[9] and spectroscopic data compared with the radiated power profile indicate that metallic radiation is not the dominant part of the total radiated power.

Thermocouple measurements indicate that disruptions deposit large amounts of energy on the bumper limiter, but normal operation does not. It is therefore expected that metals will be liberated from the surface during disruptions. Indeed several of the Inconel plates showed obvious damage due to melting (probably due to disruptions, not normal operation) when they were examined after the run period. In discharges following disruptions, there were frequently bursts of Ni, Cr, and Fe radiation. Although the largest bursts resulted in another disruption, the discharges survived most bursts, but with signs of distress. Depending on the severity of the disruption, it was often necessary to reduce the density or plasma current, or both, before operation could be reestablished at the previous parameters. Usually it required one or two shots following a disruption before the radiated power returned to its predisruption level.

Two different kinds of gettering have been tried on TFTR, the prototype bulk getter Zr-Al surface pumping system[2] and deposition of a chromium film onto about one-half of the vessel wall.[10] The activation of the Zr-Al getter panels had no effect on the plasma operation, recycling of deuterium gas or

the level of impurities observed. The total amount of gas needed to reach a given density did not appear to be influenced by the activation of six of the eight installed Zr-Al getter panels which cover about 2% of the vessel area and have a pumping speed of $120 m^3/s$. The panels were effective in reducing the base pressure in TFTR from 1×10^{-8} to 2.0×10^{-9} Torr. Twenty-eight more panels will be added to TFTR in the summer of 1985 bringing the total to 36. After the Cr deposition, Cr replaced Ni as the main metallic impurity. A reduction in the oxygen radiation was observed but no effect on the total Z_{eff} was seen at constant density. However, as Fig. 3 indicates, the density range was extended by about 20% by Cr gettering and the limiting value of Z_{eff} was lowered from about 2 to about 1.4. Note that the highest density points both with and without Cr gettering exhibit increased radiation. This is typical of discharges near the density limit and occurs at higher density in the Cr gettering case. Attempts to raise the density further resulted in disruptions in either case.

With neutral beam injection, the fractional radiated power P_{rad}/P_{tot} falls from the 40% shown in Fig. 3 for ohmic discharges to as low as 20% with 4MW injected beam power. Neutral beam injection increases Z_{eff} by 0.2 to 1.0 above that for ohmic discharges at the same density.

DISCHARGE EVOLUTION AND CONTROL

Calculations by Hawryluk and Schmidt[11] indicated that the required startup voltage for TFTR-sized tokamaks would decrease strongly with initial neutral density and that oxygen radiation would affect the discharge evolution at high neutral densities. Historically, there has been an aversion to initiation at low neutral density due to concerns about the production of runaway electrons. However, this has not been a significant problem for

TFTR. Breakdown in TFTR has occurred at initial neutral densities of 6×10^{17} to $1 \times 10^{19} m^{-3}$ (9×10^{-6} to 1.3×10^{-4} Torr prefill) and voltages of 2 to 120V/turn. Figure 4 shows the evolution of the plasma current and the applied loop voltage with and without OH interrupters at fill pressures of 3.0×10^{-5} and 1.5×10^{-5} Torr respectively. The voltage applied by the OH windings in the no-interrupter case is due to the resistive current decay in the coils aided by rectifier power supplies. In the interrupter case, the voltage is due to the resistive decay of the current through the 2.4 Ω load resistors. Plasma breakdown was achieved at 2 to 3 V/turn in the low-fill-pressure no-interrupter case. The total applied flux is shown for both cases. Analysis of discharges produced with and without interrupters at the same plasma current and major radius indicate that the flux consumption is about the same for the two cases.

The magnitude and duration of the plasma current flattop are limited by the flux available from the ohmic heating (OH) and equilibrium field (EF) windings. The poloidal flux consumption has been modelled using an analysis similar to that used by Hawryluk for PLT.[12] The applied flux is given by

$$\Phi_{ext} = M_{p-OH}\Delta I_{OH} + M_{p-EF}\Delta I_{EF} + \Phi_{eddy} \qquad (1)$$

where M_{p-OH} and M_{p-EF} are the mutual inductance between the plasma and OH and EF windings, respectively. The flux due to eddy currents Φ_{eddy} is small except early in the discharge and will be neglected. The OH coil system is precharged to $\lesssim$ 7.7Vs (24kA) before the start of the discharge and decreased to $>$ -7.7Vs ($I_{OH} > -24$kA) after the OH interrupters fire. In Fig. 5, the applied flux required to reach a given plasma current at 2.7-3.0s for R ~ 2.55m and a ~ 0.8m plasmas is shown.

Previously, an analysis of the PLT data[12] showed that the poloidal flux consumption was predominantly determined by the external and internal plasma flux. The resistive loss on axis was small. On TFTR using a similar approach, the resistive loss was also determined to be small compared to the inductive requirements. Thus, extrapolation to future larger devices should be reliable.

Active feedback control circuits are used on TFTR to control the plasma position and current. The rate of change of current in the OH coil system is used to control the plasma current which is measured by a Rogowski coil located outside the vacuum vessel. The currents in the EF and horizontal field (HF) coils are used to control the radial and vertical positions respectively. The plasma position is determined from the first moments of the poloidal field measured on a circle surrounding the plasma according to the equations[13]:

$$I_p R = [R_L + a^2 \ln(b/a)/2R_L + (b^2 - a^2)/4R_L] I_p + [2\pi(a^2 + b^2)/\mu_o] \langle \beta_p \sin\theta \rangle + [2\pi(a^2 - b^2)/\mu_o] \langle B_\theta \cos\theta \rangle \quad , \tag{2}$$

$$I_p z = [4\pi b^2/\mu_o] \langle B_p \cos\theta \rangle \quad , \tag{3}$$

where R, a and R_L, b are the major, minor radii of the plasma and field measurements respectively. The moments are formed from linear combinations of

signals from 26 B_θ and 26 B_p coils located just outside the vacuum vessel. The time-dependent minor radius, a, used in the calculation of R for the real-time signal is determined prior to the shot from the preprogrammed major radius and limiter positions. Since all the current and position coils are located outside the vacuum vessel, the signals seen by the coils must be corrected for eddy current effects. Extensive measurements of the effects of the eddy currents produced by the separate coil systems and the plasma current itself have been made. The results of these measurements are used to correct the $\langle B_p \sin\theta \rangle$, $\langle B_\theta \cos\theta \rangle$, and $\langle B_p \cos\theta \rangle$ terms. The correction to the Rogowski signal for the vacuum vessel current is the quotient of the loop voltage at the vessel wall and the vacuum vessel resistance.

Figure 6 illustrates those parts of the feedback control circuit normally used for controlling the OH, EF, and HF coil currents. The measured values of I_p, I_pR, I_pz, I_{OH}, and I_{EF} as well as their time derivatives are fed to the plasma position and current control electronics. Proportional and integral feedback are normally used for both plasma position and current control. Derivative feedback for plasma position and current as well as derivative and proportional feedback for the coil currents and beam power are available, but have not been used as yet. The spare channels are used for feedforward values for V_{OH}, V_{EF}, and V_{HF}. The plasma position and current control electronics compare the measured values to preprogrammed values, multiply the errors (and the integrated errors of I_p, I_pR, and I_pz) by time-dependent gains, and sum the products to form a voltage command to the field coils. These analog voltage signals are then sent to the power conversion computer which calculates the rectifier firing angle commands at a 1.0kHz rate. This system provides a great deal of flexibility in control of I_p, R, a, and z in TFTR.

It has been suggested that growing the plasma in minor radius such that q(a) is constant would enhance current penetration and help avoid possible hollow current profiles and unfavorable MHD activity during the current buildup.[14] The most reliable start-up on TFTR has been achieved by growing the plasmas in minor radius from the outer limiter at nearly constant safety factor q. Use of this plasma growing technique was effected by the feedback loop provided by the plasma position and current control system and the real time I_p and R measurements. For normal operation with the OH interrupters, I_p control is not effective until the rectifiers' supplies are reconnected at about 0.4s into the discharge. In this early stage I_p is determined primarily by the OH precharge, the resistance in the OH interrupter circuit, eddy current effects, the gas prefill pressure and the preprogrammed major radius. In order to grow the plasma effectively, a combination of calculation and experience is employed to produce the R(t) waveform. Figures 7 and 8 illustrate the time evolution of the gross discharge parameters for 1.8MA plasmas produced with and without the plasma growing technique, respectively. A higher rate of rise of plasma current during the slow ramp is possible in the grown plasma than in the non-grown case. The current ramp is generally more free of MHD activity in the grown than the non-grown plasmas. Note the higher radiated power and increased number of spikes in the surface voltage in the non-grown plasma. In fact, this was one of the best behaved non-grown 1.8 MA plasmas; a substantial fraction of such discharges disrupted. The small outward motion of the plasma during the current ramp in the non-grown case was deliberate: it was found that this helped avoid disruptions. It was found that attempts to reduce q to its final value in the grown plasmas more quickly than shown in Fig. 7 for $q(a) \lesssim 3.5$ were likely to end in disruption. Successful start-up was best achieved in a fairly narrow

region between constant q growth and start-up at constant major radius with no growth for low q discharges. For $q(a) \gtrsim 4$ in the flattop, growth at constant q could be used. The grown plasmas were also shrunk in minor radius during the current ramp-down. This helped to spread the heat load on the limiter. The current penetration during ramp-up has been modelled with the time-dependent transport analysis code TRANSP[15] using $T_e(R,t)$ from the electron cyclotron emission measurements. The surface voltage is matched using neoclassical resistivity and adjusting the radially constant $Z_{eff}(t)$. Figure 9 shows contours of constant q for the first 1.2 seconds of grown and non-grown 1.0MA plasmas. Note the more rapid current penetration in the grown plasma. The double valued q(r) in the non-grown case is due to a hollow $T_e(R)$ profile. Sawtooth activity is observed when the code indicates that the q=1 surface has reached about 0.1m and the calculated q=1 surface agrees with measurements of the soft X-ray inversion radius.

The plasma in TFTR can be fueled by an active gas puffing feedback system, by the injection of frozen hydrogen or deuterium pellets or by neutral beam injection. The gas injection system employs a digital feedback loop which compares the measured values of the torus pressure and the line-integral density, $n_e l$, (from either the 1mm interferometer or the far-infrared interferometer) to preprogrammed time-dependent values.[16] The errors are multiplied by time-dependent gains and summed together with a preprogrammed flow rate to form a total requested flow rate. A lookup table generated from a series of calibrated gas pulses is employed to calculate the voltage required for piezoelectric gas injection valves. Figure 10 shows the torus pressure, $n_e l$, reference $n_e l$ and calculated flow rate for a typical gas-fueled TFTR discharge. Note the slow decay of the density after the valve is turned off indicating a high recycling coefficient or long particle confinement time

τ_p. The computer also monitors the pressure of the gas plenum upstream of the piezoelectric valve to determine accurately the total gas used per shot. Gas fueling was used most frequently during the current ramp. At moderate densities, little or no gas flow is required to maintain the density. This is in contrast to PDX where gas flow rates on the order of 10T·ℓ/s were required to maintain constant density in the range of $2.5 \times 10^{19} m^{-3}$ for circular rail limiter discharges.[17,18] The total gas flow used to reach a given line average density in TFTR and PDX circular plasmas was similar, even though the TFTR plasma volume is about eight times that of PDX.

The addition of an the ORNL pellet injector[19] to TFTR in March 1985 allowed the peak density and the line average density to be increased to $1.6 \times 10^{20} m^{-3}$ and $8 \times 10^{19} m^{-3}$, respectively, without disruption. This represents a doubling of the peak density and a 40% increase in $\bar{n}_e$ beyond that achieved with D_2 gas puffing. Figure 10 shows $n_e l$ for a discharge into which 3 pellets, each containing approximately 7×10^{20} atoms of deuterium were injected at a speed of about 1200m/s. The increase in $\bar{n}_e$ of about 2×10^{19} m^{-3} for each pellet represents full accountability for the number of particles injected. The density increase for the second pellet is somewhat smaller than for the first and third. It is believed on the basis of a lower H_α signal for the second pellet that it was smaller than the first and third pellets.

Figure 10 also indicates the increase in $n_e l$ during injection of 5.3MW of deuterium neutral beams from 2.4 to 2.9s. The initial rate of density increase during neutral beam injection corresponds to the particle flux from the beams. The Hugill diagram shown in Fig. 11 summarizes the operating range of the TFTR full size ($R \sim 2.55m$, $a \sim 0.8m$) plasmas. The shaded area indicates the range for deuterium gas puffing with ohmic and neutral beam heating. The dashed line labeled B is the time history of a helium discharge up to the

maximum density. The solid line C gives a time history of a single shot with one large (2.1×10^{21} atoms) deuterium pellet. The shaded area D shows the Murakami parameter range reached with multiple small (7×10^{20} atoms) pellets. The highest values of $n_D(0)\tau_E$ and $n_D(0)\tau_E T_i(0)$ achieved thus far in TFTR are $6.5 \times 10^{19} s/m^3$ and $8 \times 10^{19} keV \cdot s/m^3$, respectively.

Near the high density limit in TFTR, a region of enhanced radiation appears in the plasma periphery. The radiation is poloidally asymmetric: the enhanced radiation generally appears on the small major radius side of the plasma near the inner wall. Both the plasma TV and the bolometer arrays observe this radiation. Along with the enhanced radiation at the edge, increases in the carbon and oxygen radiation are seen. Similar phenomena have been observed on the DIII,[20] FT,[21] ASDEX,[22] and Alcator[23] tokamaks. The Alcator C group called this phenomenon a marfe and reported no change in the bulk plasma properties due to this activity. However, on ASDEX[22] and TFTR, marfe activity is sometimes accompanied by an increase in the loop voltage and a drop in the central electron temperature measured by the scanning radiometer. Another difference on TFTR is that the location of the marfe sometimes moves up and down along the small major radius side of the plasma.

SUMMARY

This paper has described the plasma control techniques employed on TFTR. The success in reaching the plasma current and toroidal field design parameters is encouraging. The techniques used for impurity control have permitted plasma with Z_{eff} as low as 1.4 to be produced. Fuelling by pellet injection has extended the density range. During the next run period, the expected parameter range will be substantially extended with the increase of beam power to 27MW and plasma current to 3.0MA. In future experiments at

these increased parameters, impurity and discharge control will no doubt continue to play an important role.

ACKNOWLEDGMENT

This work was supported by the U.S. Department of Energy Contract No. DE-AC02-76-CHO-3073.

REFERENCES

1. W.G. Reddan, Design and Fabrication of the Vacuum Vessel for the Tokamak Fusion Test Reactor, J. Vac. Sci. Technol. 20:1173 (1982).

2. J.L. Cecchi et al., Initial Limiter and Getter Operation in TFTR, J. Nucl. Mater. 128 & 129:1 (1984).

3. M. Ulrickson et al., Performance of the TFTR Moveable Limiter Tiles, in Proc. of the 1st International Conference on Fusion Reactors Materials, Tokyo, 1984. (J. Nucl. Mater, to be published).

4. P.C. Efthimion et al., Confinement Studies of Ohmically-Heated Plasmas in TFTR, in Plasma Physics and Controlled Nuclear Fusion, IAEA, Vienna, 1984, IAEA-CN-44/A-I-2.

5. S.S. Medley et al., Periscope-Camera System for Visible and Infrared Imaging diagnostics on TFTR, Princeton Plasma Physics Laboratory Report No. PPPL-2219 (1985) accepted for publication by Rev. Sci. Instrum.

6. H.F. Dylla et al., Initial Conditioning of the TFTR Vacuum Vessel, J. Vac. Sci. Technol. A2:1188 (1984).

7. H.F. Dylla et al., First-Wall and Limiter Conditioning in TFTR, J. Nucl. Mater. 128 & 129:861 (1984).

8. H.F. Dylla, Partial Pressure Analysis of Plasmas, in Proc. IX International Vacuum Congress and V International Conference on Solid Surfaces, Madrid, 1983 (A.S.E.V.A., Madrid, 1983).

9. R.A. Hulse, Numerical Studies of Impurities in Fusion Plasmas, Nucl. Technol./Fusion 3:259 (1983).

10. H.F. Dylla et al., Chromium Getter Studies in TFTR, in Proc. 32nd National Symposium of the American Vacuum Society, Houston, 1985. (J. Vac. Sci. Technol. to be published.)

11. R.J. Hawryluk and J. Schmidt, Effects of Low-Z Impurities During the Start-up Phase of a L ge Tokamak, Nucl. Fusion 16:775 (1976).

12. R.J. Hawryluk, K. B , and D. Johnson, Volt-second Consumption During the Startup Phase of Large Tokamak, Nucl. Fusion 19:1519 (1979).

13. V.S. Mukhovatov and .D. Shafranov, Plasma Equilibrium in a Tokamak, Nucl. Fusion 11:605 ( )73).

14. D.F. Duchs, H.P. Furt , P.H. Rutherford, Skin Effects in Large Tokamaks, Nucl. Fusion 12:341 972); M. Kikuchi, Basic Principle of Constant q_a Current Build-up in Tokamaks, Princeton Plasma Physics Laboratory, Report No. PPPL-2216 1985).

15. R.J. Hawryluk, An Em rical Approach to Tokamak Transport of Plasmas in Proc. of the Cours on Physics of Plasmas Close to Thermonuclear Conditions (Varenna, taly), Report EUR-FU-BRU/XII/476/80.

16. P.H. LaMarche et al. Neutral Pressure and Gas Flow Instrumentation for TFTR, Rev. Sci. Inst n. 56:981 (1985).

17. H.F. Dylla et al., as Fueling Studies in the PDX Tokamak, J. Nucl. Mater. 121:144 (1984

18. H.F. Dylla et al., (s Fueling Studies in the PDX Tokamak II, J. Nucl. Mater. 121:144 (1984

19. S.K. Combs et al., Repeating Pneumatic Hydrogen Pellet Injector for Plasma Fueling, Rev. ci. Instrum. 56:1173 (1985).

20. D.R. Baker, R.T. Sni r and M. Nagami, Observation of Cold, High Density Plasma Near the DIII imiter, Nucl. Fusion 22:807 (1982).

21. F. Alladio et al., ne Regime of Enhanced Particle Recycling in High Density Tokamak Disc arges in the Frascati Torus, Phys. Lett. 904A:405 (1982).

22. H. Niedermeyer et al., Change of Plasma Properties Prior to High Density Disruptions in ASDEX, Max-Planck-Institut für Plasmaphysik, Garching, Report IPP-111/80 (Oct. 1983).

23. B. Lipschultz et al., Marfe: An Edge Plasma Phenomenon, Nucl. Fusion 24:977 (1984).

Table 1

TFTR PARAMETERS

	Ohmic	NBI
Toroidal Field (at 2.48m)	5.2T*	5.2T*
Plasma Current	2.5MA*	2.5MA*
Major Radius	2.1-3.1m	2.1-3.1m
Minor Radius	0.4-0.8m	0.5-0.8m
Line Average Density[a)]	$5.6 \times 10^{19} m^{-3}$	$6.2 \times 10^{19} m^{-3}$
Beam Power	--	6.3 MW

*Indicates full design parameter achieved

a) Values for D_2 gas puffing $\bar{n}_e < 8 \times 10^{19} m^{-3}$ with pellet injection.

Table 2

TYPICAL DISCHARGE CLEANING PARAMETERS

	GDC	PDC Low I_p	PDC High I_p
H_2 Pressure	5-6mTorr	(1-4) x 10^{-4}Torr	(1-4) x 10^{-5}Torr
Discharge Current	15A	20-50kA	100-200kA
Discharge Duration	continuous	≤50ms	40-100ms
Repetition Period	continuous	4.5-10s	4.5-10s
Toroidal Field	0	≲ 0.4T	0.4-0.6T
Discharge Voltage	390 V (dc)	≲ 50V/turn	≲ 50V/turn

FIGURE CAPTIONS

FIG. 1 Total power radiated for the different major radius programming discussed in the text.

FIG. 2. Density dependence of central relative Ni concentration at different times after PDC. The Ni concentration at constant density varied as $N^{-0.6}$ where N is the number of shots since PDC.

FIG. 3. The fractional radiated power versus line average density with and without Cr gettering. This shows the power radiated rising as the density limit is approached in either case.

FIG. 4. The time evolution during the discharge initiation of the applied voltage, plasma current, and applied flux for two different discharges. The left half shows a discharge made without using the OH interrupters and at a prefill pressure of 1.5×10^{-5}Torr, while the discharge shown on the right employs the OH interrupters with a 2.4Ω load resistance and a prefill of 3.0×10^{-5}Torr.

FIG. 5. The applied flux as a function of plasma current for large minor radius TFTR plasmas.

FIG. 6. A block diagram of the plasma position and current control electronics used. Coil currents, beam power, and time derivatives are also available, but have not as yet been used. The bars over variables denote a reference value. The symbols F, G, and H denote

time-dependent preprogrammed gains for the horizontal field, equilibrium field and ohmic heating windings. The outputs are voltage requests made to the power conversion computer.

FIG. 7. Parameters for a 1.8MA plasma produced using the growing technique discussed in the text.

FIG. 8. Parameters of a 1.8MA non-grown plasma for comparison with Fig. 7. The small change in R at 1 to 1.5 seconds was intentional.

FIG. 9. TRANSP modelling of current diffusion for grown and non-grown plasmas using $T_e(R,t)$ from electron cyclotron emission measured by the heterodyne radiometer. V_s from the code was matched to the measured V_s by using neoclassical resistivity and adjusting $Z_{eff}(t)$.

FIG. 10. Density fueling by gas puffing, pellet injection, and neutral beams. The gas puffing feedback system is discussed in the text. The pellets used in the pellet injection case were $7 \times 10^{}$ atoms. The beam injection case was 5.3MW of D^0.

FIG. 11 Hugill diagram for TFTR plasmas.

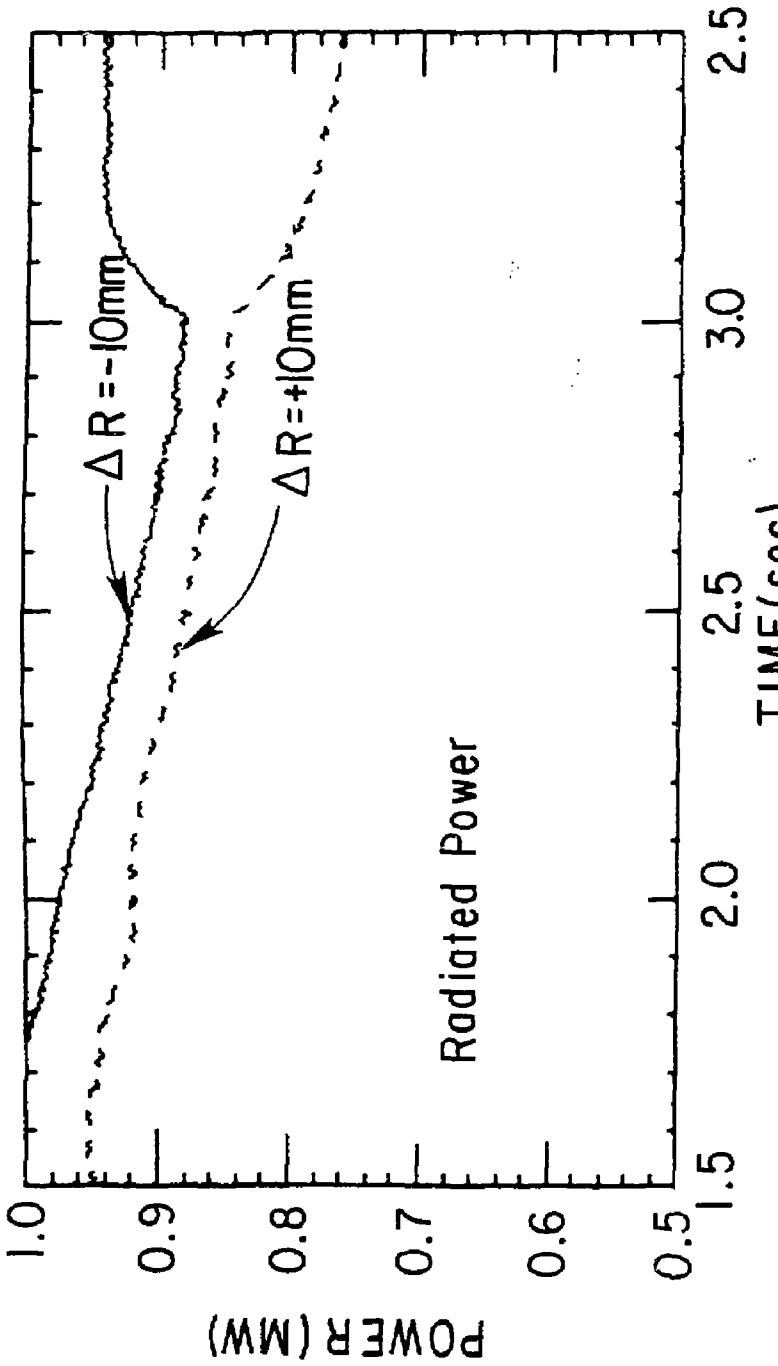
ΔR=-10mm
ΔR=+10mm
Radiated Power
POWER (MW)
TIME(sec)
1.0
0.9
0.8
0.7
0.6
0.5
1.5
2.0
2.5
3.0
2.5

Fig. 1

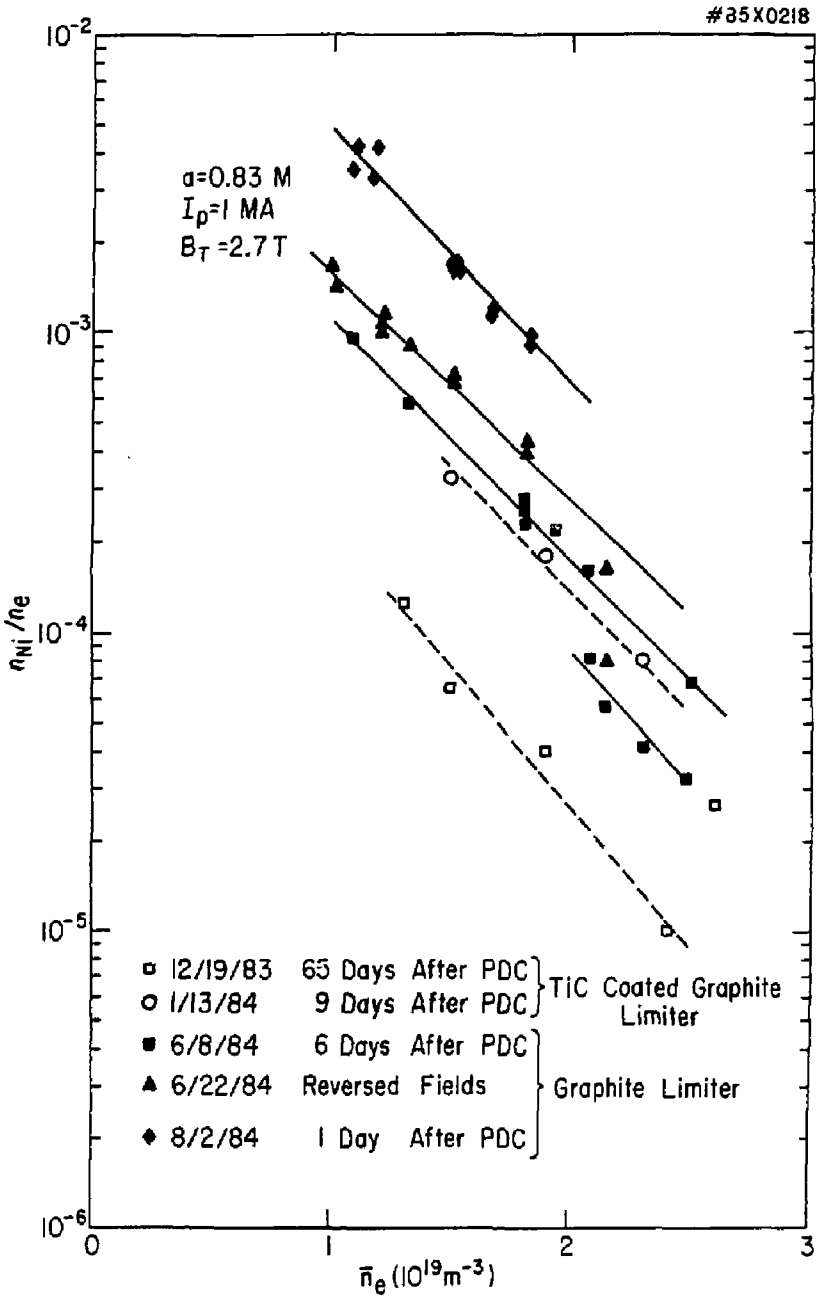
#85X0218
a=0.83 M
I_p=1 MA
B_T =2.7 T
n_{Ni}/n_e
$\bar{n}_e$ (10^{19}m^{-3})
12/19/83 63 Days After PDC
1/13/84 9 Days After PDC
TiC Coated Graphite Limiter
6/8/84 6 Days After PDC
6/22/84 Reversed Fields
8/2/84 1 Day After PDC
Graphite Limiter

Fig. 2

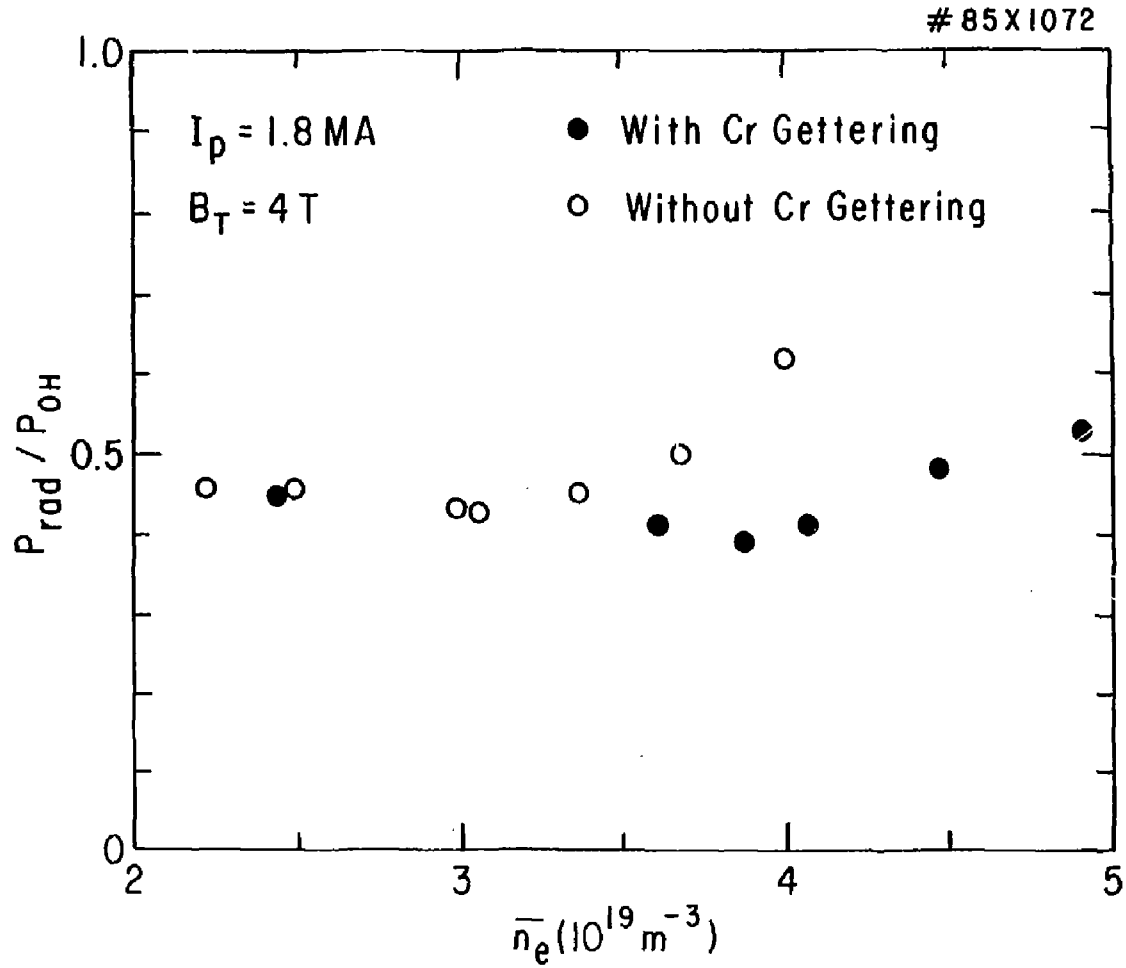
#85X1072
1.0
0.5
0
I_p = 1.8 MA
B_T = 4 T
With Cr Gettering
Without Cr Gettering
P_{rad} / P_{OH}
2
3
4
5
$\bar{n}_e (10^{19} m^{-3})$

Fig. 3

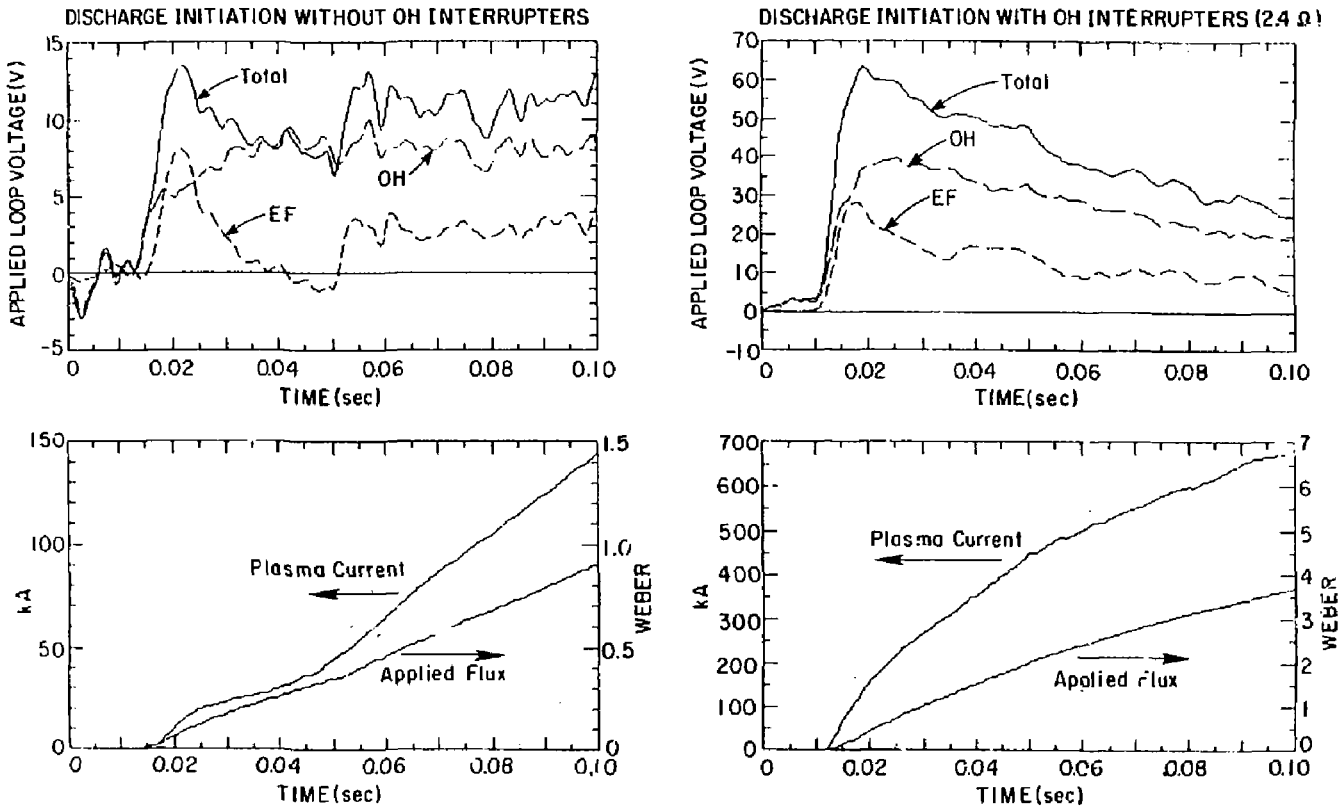
DISCHARGE INITIATION WITHOUT OH INTERRUPTERS
APPLIED LOOP VOLTAGE(V)
Total
OH
EF
TIME(sec)
DISCHARGE INITIATION WITH OH INTERRUPTERS (2.4 Ω)
APPLIED LOOP VOLTAGE (V)
Total
OH
EF
TIME(sec)
kA
WEBER
Plasma Current
Applied Flux
TIME(sec)
kA
WEBER
Plasma Current
Applied Flux
TIME(sec)

Fig. 4

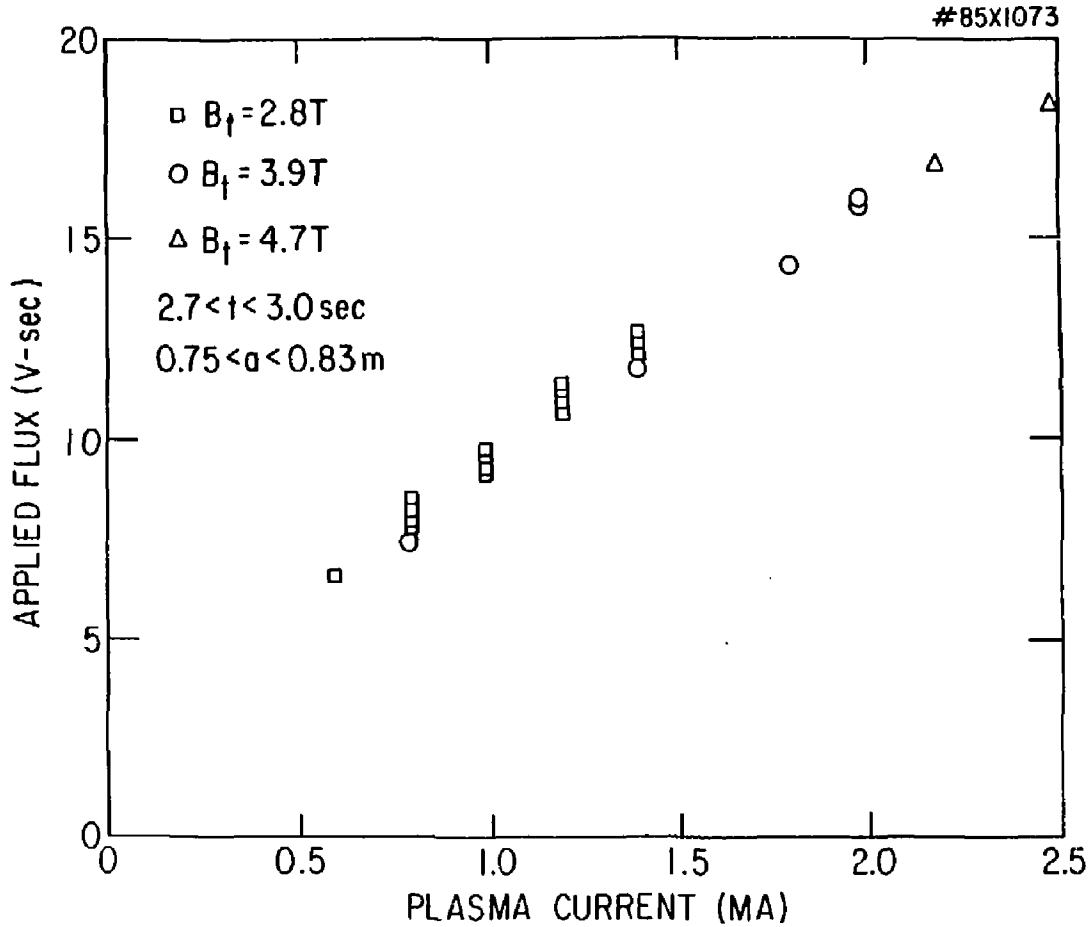
#85X1073
20
15
10
5
0
0
0.5
1.0
1.5
2.0
2.5
APPLIED FLUX (V-sec)
PLASMA CURRENT (MA)
□ B_t = 2.8T
○ B_t = 3.9T
△ B_t = 4.7T
2.7 < t < 3.0 sec
0.75 < a < 0.83 m

Fig. 5

#85X1093

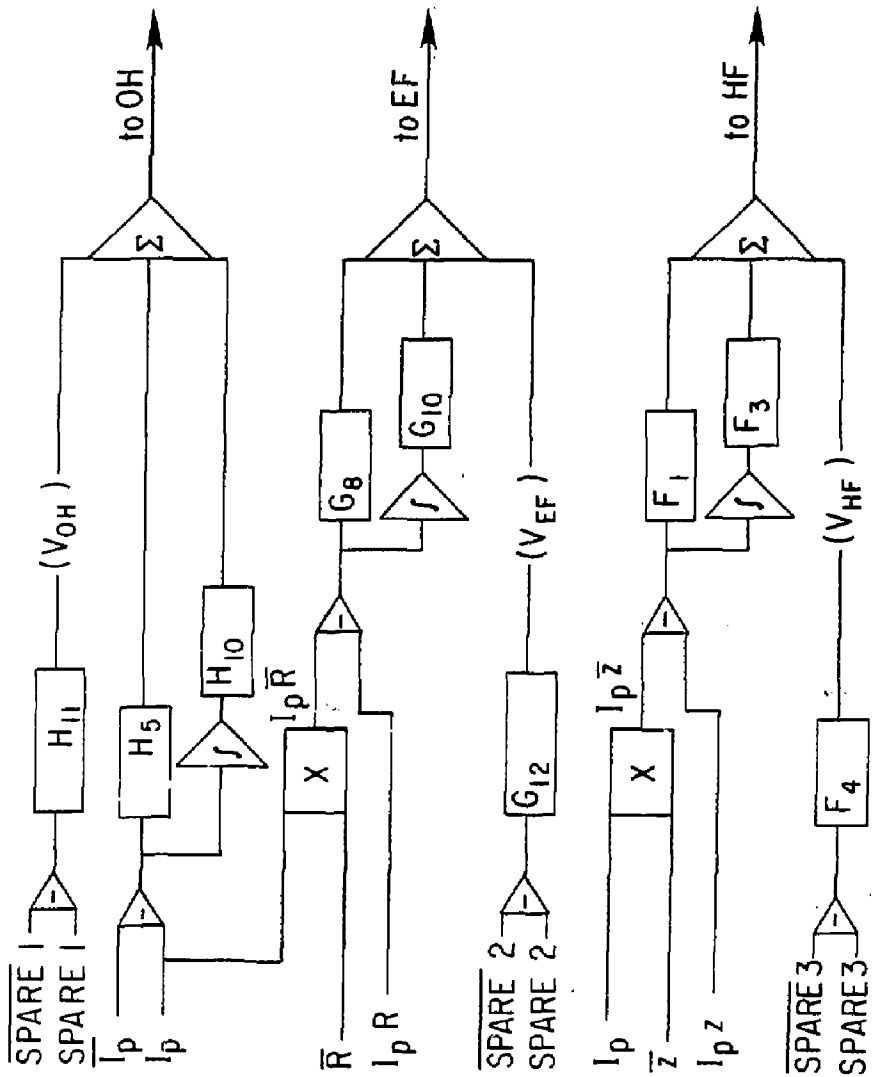

Fig. 6

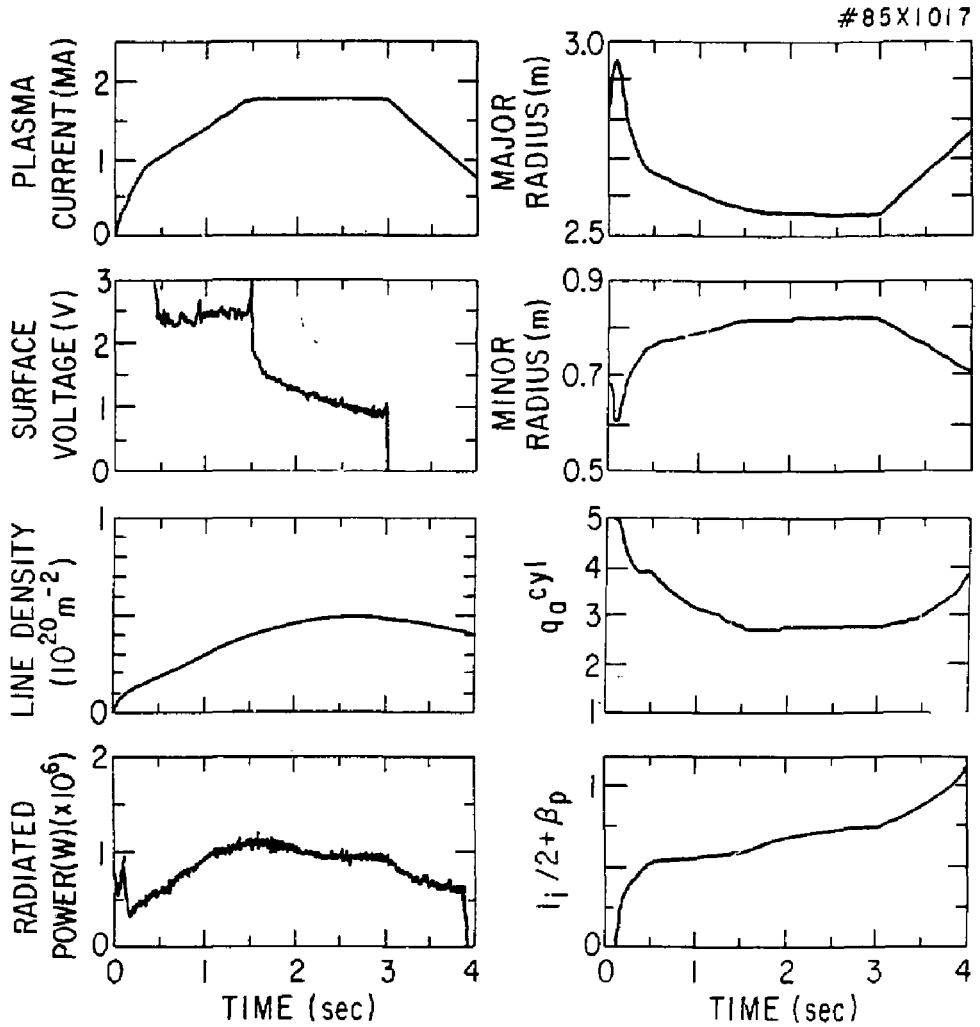
#85X1017
PLASMA CURRENT (MA)
MAJOR RADIUS (m)
SURFACE VOLTAGE (V)
MINOR RADIUS (m)
LINE DENSITY (10^{20} m^{-2})
q_a^{cyl}
RADIATED POWER (W) (x 10^6)
$l_i/2+\beta_p$
TIME (sec)
TIME (sec)

Fig. 7

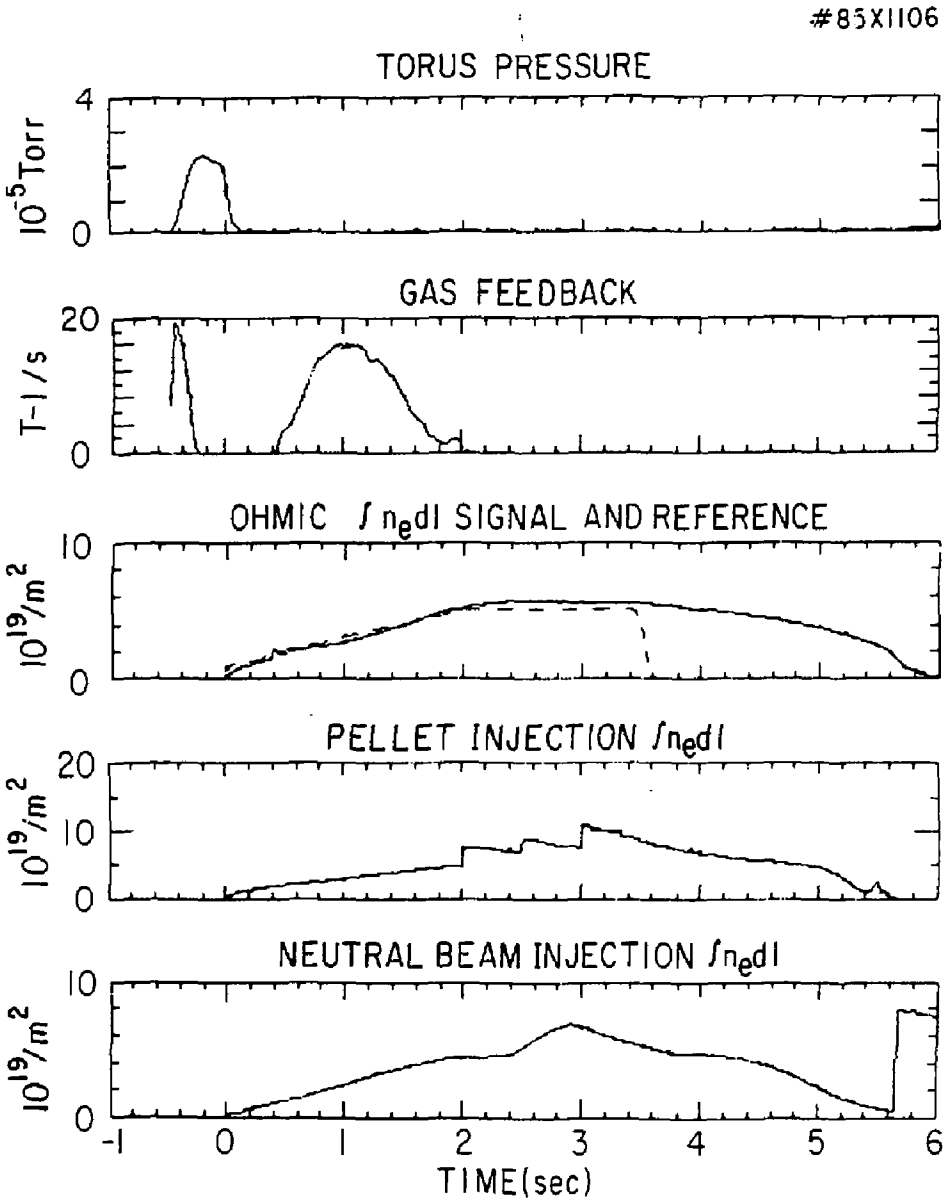
#85X1106
TORUS PRESSURE
10^{-5}Torr
4
0
GAS FEEDBACK
T-l/s
20
0
OHMIC $\int n_e dl$ SIGNAL AND REFERENCE
$10^{19}/m^2$
10
0
PELLET INJECTION $\int n_e dl$
$10^{19}/m^2$
20
10
0
NEUTRAL BEAM INJECTION $\int n_e dl$
$10^{19}/m^2$
10
0
-1
0
1
2
3
4
5
6
TIME(sec)

Fig. 9

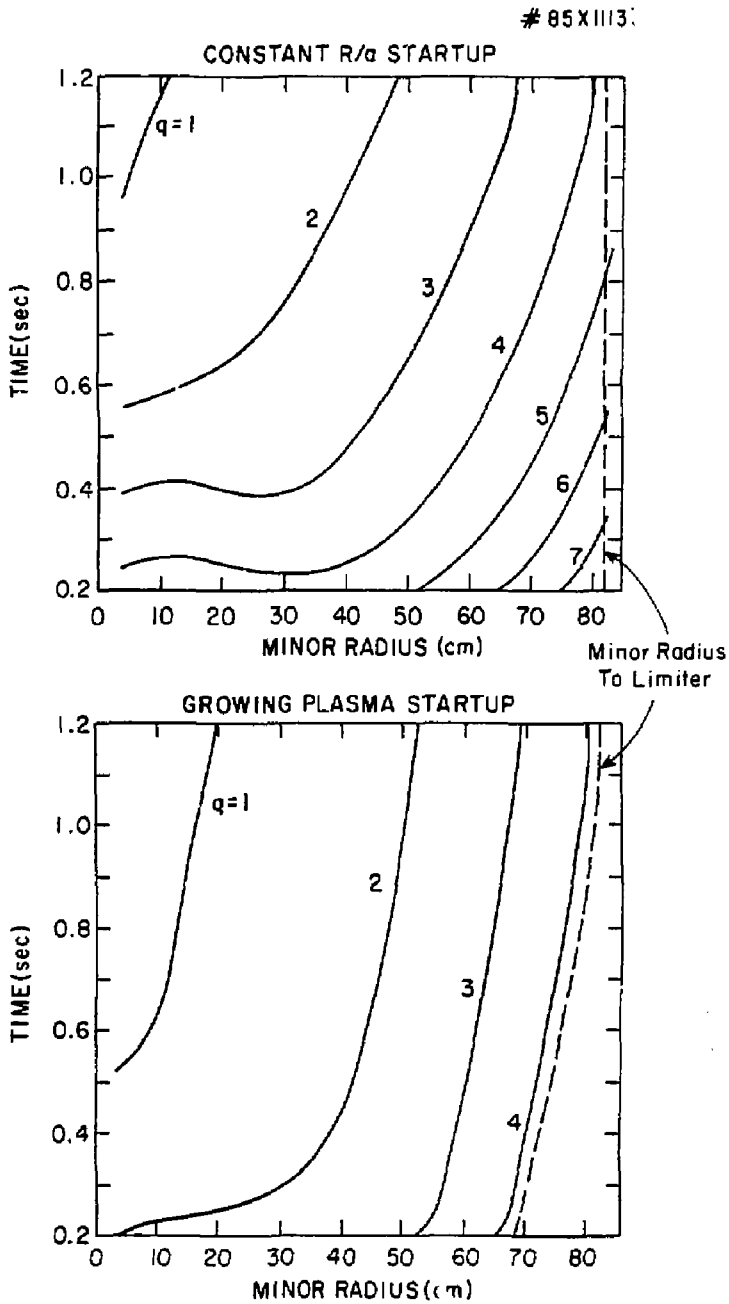
#85X1113
CONSTANT R/a STARTUP
TIME(sec)
MINOR RADIUS (cm)
q=1
2
3
4
5
6
7
Minor Radius
To Limiter
GROWING PLASMA STARTUP
TIME(sec)
MINOR RADIUS (cm)
q=1
2
3
4

Fig. 9

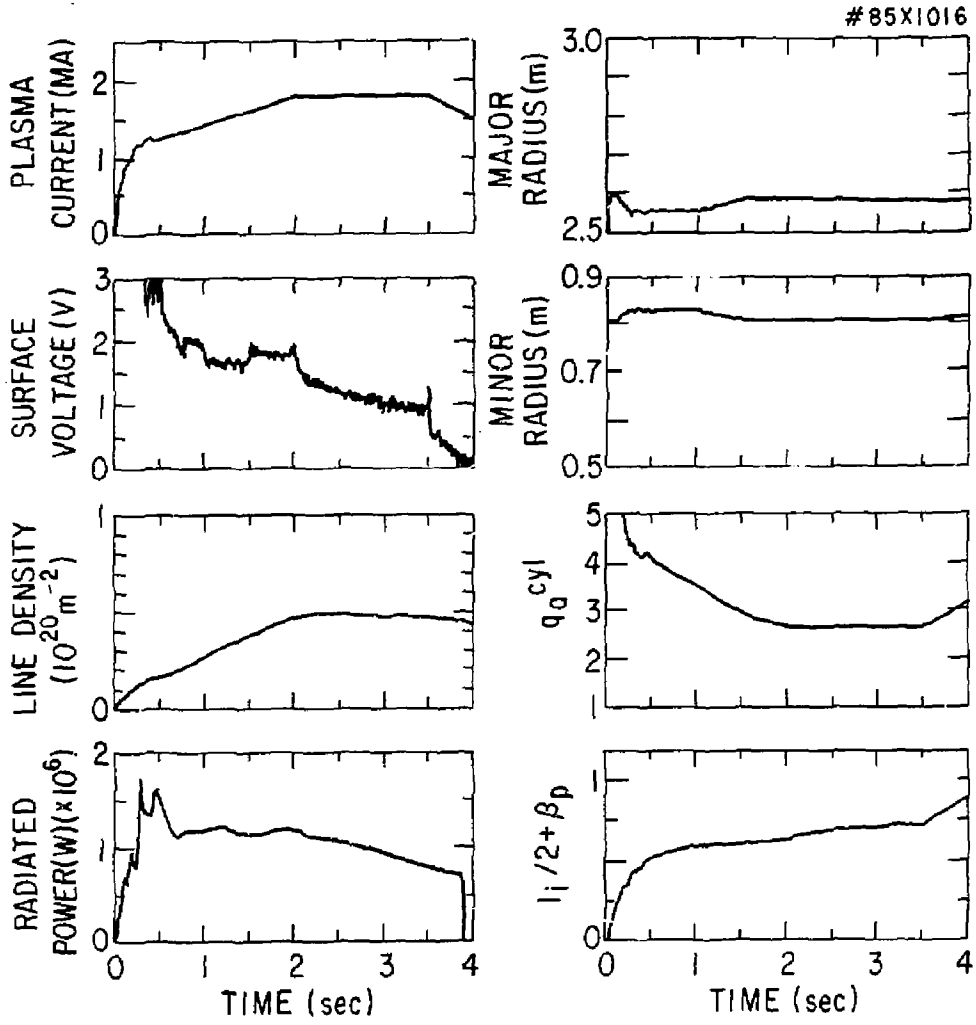
#85X1016
PLASMA CURRENT (MA)
MAJOR RADIUS (m)
SURFACE VOLTAGE (V)
MINOR RADIUS (m)
LINE DENSITY (10^{20} m^{-2})
q_a^{cyl}
RADIATED POWER(W)(x10^6)
$l_i/2+\beta_p$
TIME (sec)
TIME (sec)

Fig. 1a

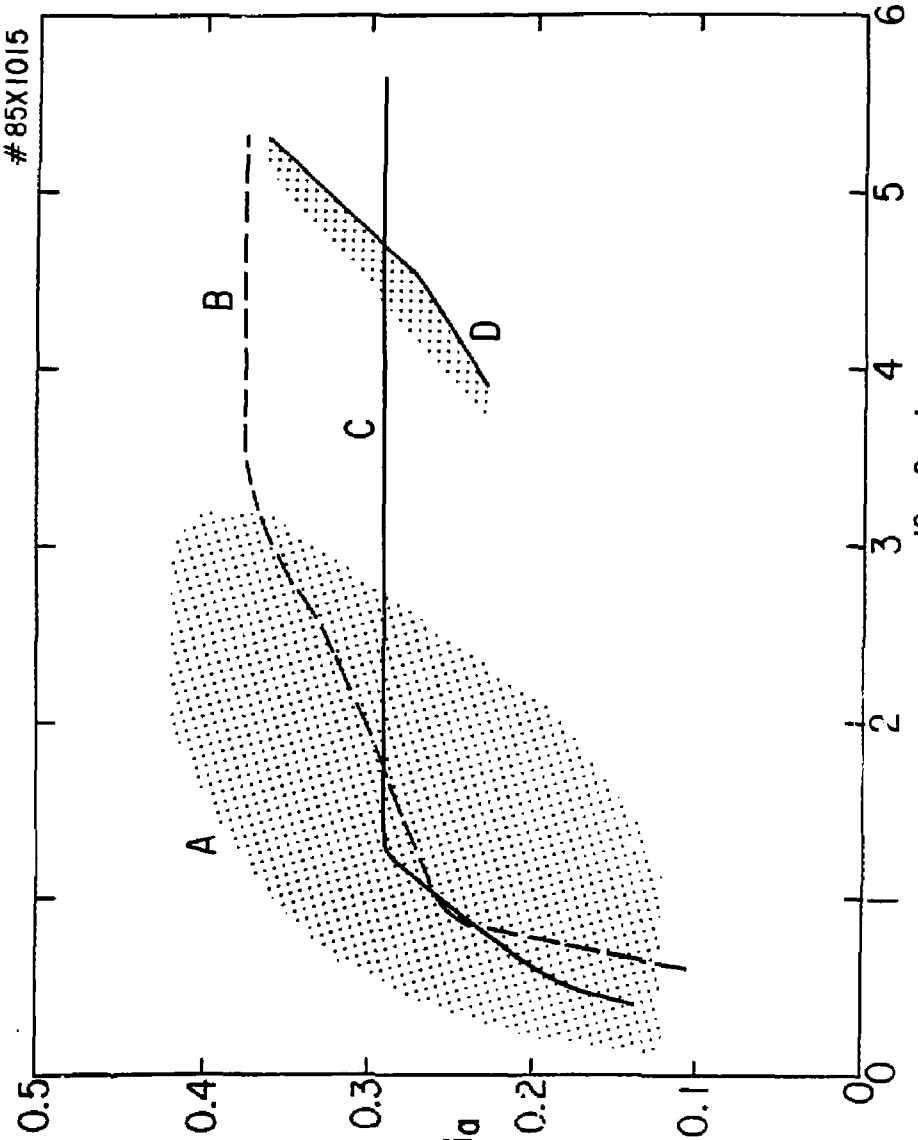

Fig. 11

EXTERNAL DISTRIBUTION IN ADDITION TO UC-20

Plasma Res Lab, Austra Nat'l Univ, AUSTRALIA
Dr. Frank J. Paoloni, Univ of Wollongong, AUSTRALIA
Prof. I.R. Jones, Flinders Univ., AUSTRALIA
Prof. M.H. Brennan, Univ Sydney, AUSTRALIA
Prof. F. Cap, Inst Theo Phys, AUSTRIA
Prof. Frank Verheest, Inst theoretische, BELGIUM
Dr. D. Palumbo, Dg XII Fusion Prog, BELGIUM
Ecole Royale Militaire, Lab de Phys Plasmas, BELGIUM
Dr. P.H. Sakanaka, Univ Estadual, BRAZIL
Dr. C.R. James, Univ of Alberta, CANADA
Prof. J. Teichmann, Univ of Montreal, CANADA
Dr. H.M. Skarsgard, Univ of Saskatchewan, CANADA
Prof. S.R. Sreenivasan, University of Calgary, CANADA
Prof. Tudor W. Johnston, INRS-Energie, CANADA
Dr. Hannes Barnard, Univ British Columbia, CANADA
Dr. M.P. Bachynski, MPB Technologies, Inc., CANADA
Chalk River, Nucl Lab, CANADA
Zhengwu Li, SW Inst Physics, CHINA
Library, Tsing Hua University, CHINA
Librarian, Institute of Physics, CHINA
Inst Plasma Phys, Academia Sinica, CHINA
Dr. Peter Lukac, Komenskeho Univ, CZECHOSLOVAKIA
The Librarian, Culham Laboratory, ENGLAND
Prof. Schatzman, Observatoire de Nice, FRANCE
J. Radet, CEN-BP6, FRANCE
AM Dupas Library, AM Dupas Library, FRANCE
Dr. Tom Mual, Academy Bibliographic, HONG KONG
Preprint Library, Cent Res Inst Phys, HUNGARY
Dr. R.K. Chhajlani, Vikram Univ. INDIA
Dr. B. Dasgupta, Saha Inst, INDIA
Dr. P. Kaw, Physical Research Lab, INDIA
Dr. Phillip Rosenau, Israel Inst Tech, ISRAEL
Prof. S. Cuperman, Tel Aviv University, ISRAEL
Prof. G. Rostagni, Univ Di Padova, ITALY
Librarian, Int'l Ctr Theo Phys, ITALY
Miss Clelia De Palo, Assoc EURATOM-ENEA, ITALY
Biblioteca, del CNR EURATOM, ITALY
Dr. M. Yamato, Toshiba Res & Dev, JAPAN
Direc. Dept. Lg. Tokamak Dev. JAERI, JAPAN
Prof. Nobuyuki Inoue, University of Tokyo, JAPAN
Research Info Center, Nagoya University, JAPAN
Prof. Kyoji Nishikawa, Univ of Hiroshima, JAPAN
Prof. Sigeru Mori, JAERI, JAPAN
Prof. S. Tanaka, Kyoto University, JAPAN
Library, Kyoto University, JAPAN
Prof. Ichiro Kawakami, Nihon Univ, JAPAN
Prof. Satoshi Itoh, Kyushu University, JAPAN
Dr. D.I. Choi, Adv. Inst Sci & Tech, KOREA
Tech Info Division, KAERI, KOREA
Bibliotheek, Fom-Inst Voor Plasma, NETHERLANDS
Prof. B.S. Liley, University of Waikato, NEW ZEALAND
Prof. J.A.C. Cabral, Inst Superior Tecn, PORTUGAL
Dr. Octavian Petrus, ALI CUZA University, ROMANIA
Prof. M.A. Hellberg, University of Natal, SO AFRICA
Dr. Johan de Villiers, Plasma Physics, Nucor, SO AFRICA
Fusion Div. Library, JEN, SPAIN
Prof. Hans Wilhelmson, Chalmers Univ Tech, SWEDEN
Dr. Lennart Stenflo, University of UMEA, SWEDEN
Library, Royal Inst Tech, SWEDEN
Centre de Recherchesen, Ecole Polytech Fed, SWITZERLAND
Dr. V.T. Tolok, Khaikov Phys Tech Ins, USSR
Dr. D.D. Ryutov, Siberian Acad.Sci, USSR
Dr. G.A. Eliseev, Kurchatov Institute, USSR
Dr. V.A. Glukhikh, Inst Electro-Physical, USSR
Institute Gen. Physics, USSR
Prof. T.J.M. Boyd, Univ College N Wales, WALES
Dr. K. Schindler, Ruhr Universitat, W. GERMANY
Nuclear Res Estab, Julich Ltd, W. GERMANY
Librarian, Max-Planck Institut, W. GERMANY
Bibliothek, Inst Plasmaforschung, W. GERMANY
Prof. R.K. Janev, Inst Phys, YUGOSLAVIA